ELSEVIER

International Journal of Solids and Structures 40 (2003) 7245–7268

INTERNATIONAL JOURNAL OF SOLIDS and STRUCTURES

www.elsevier.com/locate/ijsolstr

A coupled interface-multilayer approach for mixed mode delamination and contact analysis in laminated composites

Domenico Bruno *, Fabrizio Greco, Paolo Lonetti

Department of Structural Engineering, University of Calabria, Via P. Bucci, Cubo 39C, 87030 Rende Cosenza, Italy

Received 2 September 2003; received in revised form 2 September 2003

Abstract

An accurate laminate model developed by using multilayer shear deformable plate modeling and interface elements, based on fracture mechanics and contact mechanics, is proposed to analyze mixed mode delamination in composite laminates. Perfect adhesion along the undelaminated portion of the delamination plane is simulated by treating interface stiffnesses as penalty parameters, whereas to enforce interface displacement continuity between plate elements constituting each sub-laminate above or below the delamination plane, the Lagrange multiplier method is used. The governing differential equations are derived through a variational procedure by using a modified total potential energy functional. Results are obtained by numerical integration of the non-linear three-point boundary value problem modeling mixed-mode delamination of the laminate plate subjected to end loading, which accounts also for the frictionless contact condition.

The coupling of a penalty procedure with the Lagrange multiplier method, results in an accurate and direct energy release rate evaluation. Comparisons with results available from the literature obtained with a local continuum approach, show that mode partition may be performed to the desired accuracy by refining multilayer plate models for each sub-laminate. In addition, original analytical formulas for mode partition are obtained by coupling the interface approach and fracture mechanics concepts, evidencing the effectiveness of the proposed approach and gaining a better insight into the influence of shear effects on mode decomposition. Numerical computations for practical problems, evidence both the relative simplicity and the efficiency of the proposed model to represent mixed mode interlaminar fracturing as well as crack–face interaction.

Keywords: Laminates; Delamination; Multilayer; Interface; Mode partition; Contact

1. Introduction

Classic delamination models based on plate theories, which are frequently adopted in the literature, are very useful to obtain an accurate estimate of total energy release rate. According to these models, delamination analysis is carried out by considering the laminate as composed of two plate elements in the

* Corresponding author. Tel.: +39-984-496914; fax: +39-984-494045.
E-mail address: d.bruno@unical.it (D. Bruno).

0020-7683/$ - see front matter © 2003 Elsevier Ltd. All rights reserved.
doi:10.1016/j.ijsolstr.2003.09.006

delaminated and a single plate element in the undelaminated region (see, for instance, Cochelin and Potier-Ferry, 1991; Storåkers and Andersson, 1988; Williams, 1988; Kim, 1997; Kouchakzadeh and Sekine, 2000; Bruno and Greco, 2000; Chai et al., 1981). On the other hand, classic delamination models may provide inaccurate results especially when utilized to evaluate energy release rate mode components. As a consequence, a notable underestimation of the actual energy release rate mode components may arise since shear effects are usually neglected and the local crack tip strain state is not accurately estimated.

To obtain an accurate mode partition, a continuum formulation is often required (see, for instance, Hutchinson and Suo, 1992; Schapery and Davidson, 1990). According to this methodology, mode partition is developed at first by calculating the total energy release rate by using the classic plate theory and, secondly, completing mode decomposition by numerical solutions of the local continuum model which substitutes plate kinematics assumptions in a short plate element containing the delamination front, treated as a semi-infinite crack scheme. This procedure may lead to the extraction of semi-analytical expressions for energy release rate mode components (Suo, 1990; Suo and Hutchinson, 1990; Davidson et al., 1995), in which shear effects are neglected. On the other hand, these effects can be taken into account in an approximate way by correcting stress intensity factors (Nilsson et al., 2001a). However some other complications may arise. As a matter of fact, for schemes whose complexity is increased due to anisotropic properties, layup sequence and geometry, the local computation may become computationally expensive and additional difficulties may be encountered due to the classic oscillatory singularity (Raju et al., 1988). Moreover, some approximations may be needed to transfer the local problem results to the overall delamination analysis.

To this end, an intermediate approach between classic delamination models and that based on a local continuum analysis, based on the interface element concept, has been proposed (Ascione and Bruno, 1985; Allix et al., 1995; Allix and Corigliano, 1996; Point and Sacco, 1996; Bui et al., 2000). Interface models when used in conjunction with plate theories, while retaining the simplicity of classic delamination models, lead to an accurate and self-consistent delamination analysis. In addition they are able to account for nonlinear effects due to bridging mechanisms (Greco et al., 2002) or to damage and can easily incorporate the unilateral contact condition.

The main objective of this paper is to asses the reliability of interface models, which have shown their effectiveness and simplicity in determining total energy release rate and in incorporating transverse shear effects (Bruno and Greco, 2001a,b), to derive mode partition. To this aim, the accuracy of fracture mode partition obtained by interface models will be investigated in comparison with results obtained by using a local continuum approach. This theoretical investigation would make a contribution to fill the gap between continuum models and simplified models based on plates theories, used in delamination analysis and would give a better insight into the influence of shear effects on mode partition, which has been frequently neglected in models based on a local continuum approach. To this end, the interface model used in conjunction with a first order shear deformable two-layer plate introduced in (Bruno and Greco, 2001a,b), is here extended to a multilayer formulation in order to account for a more accurate description of the local crack tip strain state and to incorporate contact analysis. Linear interface elements lead to a direct computation of energy release rate mode components. The solution procedure, based on a numerical integration scheme, utilizes the Lagrange multiplier and the penalty methods and accounts also for unilateral frictionless contact by using a contact interface model.

Results obtained for two-dimensional delamination schemes show that the proposed model may be a useful alternative to both methods based on a local continuum analysis and/or on the virtual crack closure technique (VCCT). Generally speaking, the coupling between a plate formulation and the physical interface model, which may be interpreted as a very thin layer embedding delamination, circumvents the classic oscillatory problem and gives a better understanding of transverse shear influence on mode decomposition. Specifically, for the problems considered here, the present methodology avoids the need for any additional computation since is able to predict accurately mode separation directly in the stress analysis of the whole

delaminated plate. On the other hand, for schemes that are more complex due to its geometrical and non-linear characteristics, where the splitting into a global and local problem can be a more versatile approach (Nilsson et al., 2001b), the proposed model can be efficiently used in the context of a local analysis to compute directly mode partition, whereas continuum approaches may require more complex calculations based on solid finite elements to capture the three-dimensional problem behavior. Extension of the present analysis to more complex delamination problems (multiple delaminations, delamination buckling and general geometries) will be object of future investigations.

2. Description of delaminated plate model

The model to be analyzed consists of a laminate plate composed of unidirectional fibre reinforced plies and containing a single initial through-the-width delamination of length a, which separates the laminated plate in two sub-laminates. The upper sub-laminate thickness is denoted with h_1, whereas the lower sub-laminate thickness is denoted with h_2. The model is illustrated in Fig. 1. Assuming that the laminate width B is large if compared to the x–y plane region affected by the local crack tip strain state, and constant loading conditions along the width direction, a plane strain state may be considered. Arbitrary orientations of fibres in plies may originate a small mode III energy release rate component, which is here neglected. A linear interface model is introduced along the undelaminated portion of the delamination plane, whose constitutive relationship has the form:

$$\sigma_{yy} = k_{yy}\Delta w, \quad \sigma_{yx} = k_{yx}\Delta u, \tag{1}$$

which relates the components of the interface traction vector, σ_{yy} and σ_{yx} in the normal (y) and tangential (x) directions, respectively, and the corresponding relative interface displacements, Δw and Δu. This leads to a direct mode decomposition through the following formulas:

$$G_{\mathrm{I}} = \begin{cases} \lim\limits_{k_{yx},k_{yy}\to\infty} \frac{1}{2}k_{yy}\Delta w^2 & \Delta w \geqslant 0 \\ 0 & \Delta w < 0 \end{cases}, \quad G_{\mathrm{II}} = \lim_{k_{yx},k_{yy}\to\infty} \frac{1}{2}k_{yx}\Delta u^2, \tag{2}$$

as proved in (Bruno and Greco, 2001a,b). In Eq. (2), Δu and Δw are evaluated at the delamination front and k_{yy}, k_{yx} represent the interface stiffness parameters, treated as penalty parameters. When interpenetration of delaminated plate members happens, a pure mode II condition is assumed. To prevent interpenetration between delaminated sub-laminates, a unilateral frictionless contact interface is introduced along the delaminated domain of the interface, characterized by a zero stiffness for opening relative displacements ($\Delta w \geqslant 0$) and a positive stiffness for closing relative displacements ($\Delta w < 0$). To this end the following extended interface model, whose constitutive law is valid both for undelaminated and delaminated interface domains, is introduced:

$$\sigma_{yy} = \left[1 - \frac{1}{2}d(1 + \mathrm{sign}(\Delta w))\right]k_{yy}\Delta w, \quad \sigma_{yx} = (1-d)k_{yx}\Delta u, \tag{3}$$

where d is a damage variable, taking the value 1 value for no adhesion and the value 0 for perfect adhesion and sign is the signum function. In addition σ_{yy} is the contact stress, k_{yy} is the penalty number imposing contact constraint and sign is the signum function. When $d = 1$ a contact interface is obtained and σ_{yy} is the contact stress, whereas k_{yy} is the penalty number imposing contact constraint. A very large stiffness restricts sub-laminate overlapping and simulates contact condition.

The laminate is schematized by a multilayer plate model and, therefore, the upper sub-laminate is divided into n_u plate elements whereas the lower one into n_l plate elements (see Fig. 1). Each plate element may, in turn, represent one or several physical fibre-reinforced plies and is governed by the first order shear

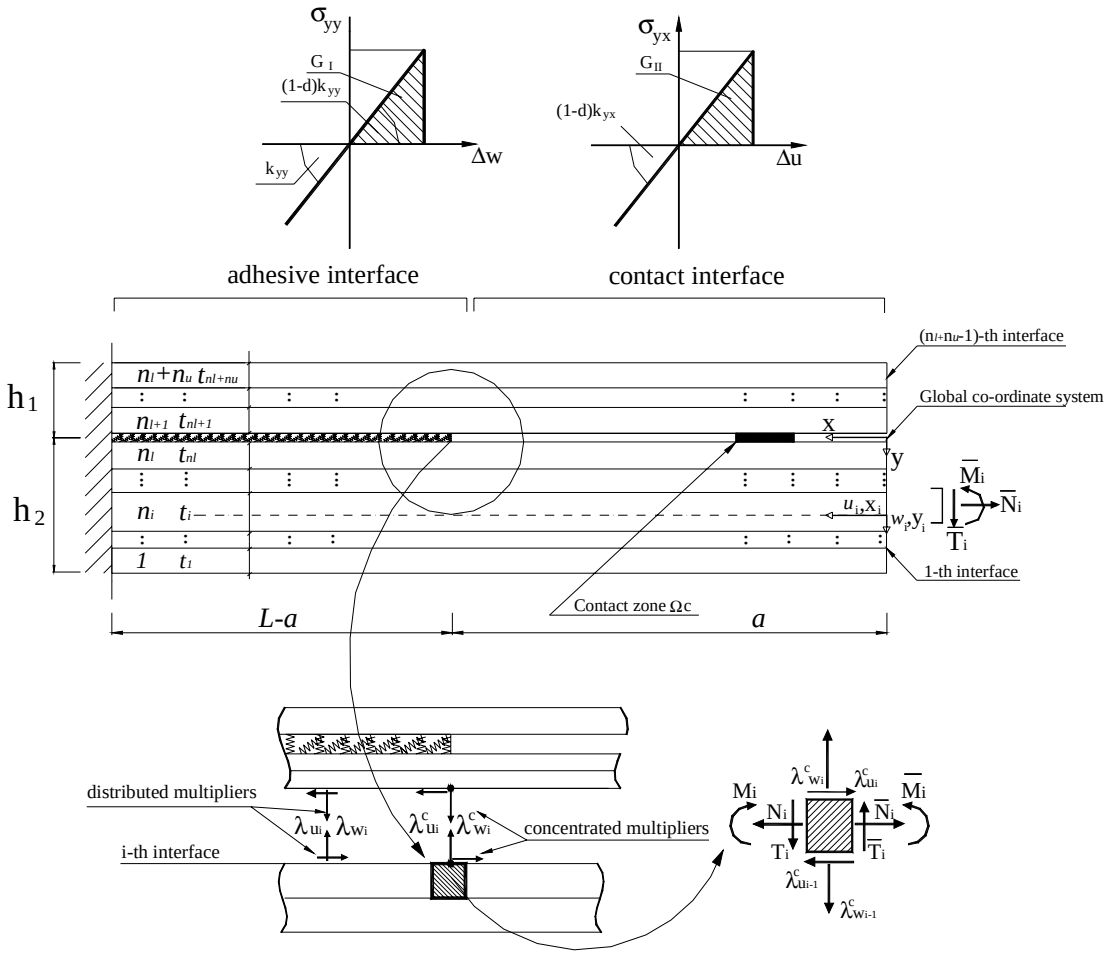

Fig. 1. Delaminated laminate and interface models simulating contact and interlaminar damage. In addition distributed and concentrated Lagrange multipliers arising from stress singularities in the laminate structure, are shown.

deformation theory. The thickness of the ith plate element is denoted by t_i. The membrane strain at the reference surface, the curvature and transverse shear strains, respectively, are defined as:

$$\varepsilon_i = u_i', \quad \kappa_i = \psi_i', \quad \gamma_i = \psi_i + w_i',$$

where $u_i(x_i)$ and $w_i(x_i)$ are the mid-surface in-plane and transverse displacements, respectively, $\psi_i(x_i)$ denotes rotations of transverse normals, and a prime denotes the derivative with respect to x_i. The constitutive relations between stress resultants and corresponding strains are:

$$\begin{Bmatrix} N_i \\ M_i \end{Bmatrix} = \begin{bmatrix} A_i & B_i \\ B_i & D_i \end{bmatrix} \begin{Bmatrix} \varepsilon_i \\ \kappa_i \end{Bmatrix}, \quad T_i = H_i \gamma_i, \tag{4}$$

where N_i is the membrane force resultant, M_i the moment resultant and T_i the transverse shear force resultant. In addition, A_i, D_i, B_i and H_i denotes the classical extensional, bending, bending-extensional coupling and shear stiffnesses. Displacement continuity requirement along an undamaged interface com-

prised between two adjacent plate elements, is imposed by means of a constraint functional introducing opportune Lagrange multipliers.

3. Theoretical formulation

Assume a quasi-static delamination growth for the laminated plate. For simplicity, consider that the plate is loaded by edge forces on one side and with clamped boundary conditions on the other side, as illustrated in Fig. 1. Governing equilibrium equations will be derived through a variational approach, via the minimization condition of a modified total potential energy functional for unit width Π_k, which includes interface displacement continuity by means of constraint functionals using opportune Lagrange multipliers and adhesion and frictionless contact constraints, by using a penalty functionals. The modified total potential energy functional for unit width of the laminate, can be expressed as follows

$$\Pi_k(u_i, w_i, \psi_i) = U + I + L - W, \tag{5}$$

where U is the strain energy of the whole plate, I the interface penalty functional, L the Lagrange functional constraint for adhesion between undamaged layers and W is the work of the external loads. In particular, U, I and L assume the following expressions:

$$\begin{aligned} U &= \sum_{i=1}^{n_u+n_l} \int_0^L [\Phi_i(u_i, w_i, \psi_i)]\,\mathrm{d}x, \quad I = \int_0^L (\sigma_{yy}\Delta w_{n_l} + \sigma_{yx}\Delta u_{n_l})\,\mathrm{d}x, \\ L &= \sum_{j=1}^{n_l+n_u-1} \int_0^L [\lambda_{u_j}\Delta u_j + \lambda_{w_j}\Delta w_j]\,\mathrm{d}x \quad j \neq n_l, \end{aligned} \tag{6}$$

where $\Phi_i = 1/2(N_i\varepsilon_i + M_i\kappa_i)$ is the strain energy density of the ith plate element; I is expressed in terms of the relative opening and sliding interface displacements, $\Delta w_{n_l} = w_{n_l} - w_{n_l+1}$, $\Delta u_{n_l} = u_{n_l} - u_{n_l+1}$, evaluated at the interface between the n_lth and the $n_l + 1$th plate elements (which is therefore denoted as the n_lth interface) and in terms of σ_{yy}, σ_{yx}, defined in Eq. (3); Δu_j and Δw_j in the expression of L denote relative displacements at the jth interface between the jth and the $j + 1$th plate element:

$$\begin{cases} \Delta u_j = u_j - \frac{t_j}{2}\psi_j - u_{j+1} - \frac{t_{j+1}}{2}\psi_{j+1} \\ \Delta w_j = w_j - w_{j+1} \end{cases} \quad j = 1, \ldots, n_u + n_l - 1, \tag{7}$$

and λ_{u_j} and λ_{w_j} denote Lagrange multipliers representing interlaminar stresses at the jth interface. In Eq. (5) the subscript k denotes dependence on the penalty parameters and plate elements are numerated starting from the lowest one.

The equilibrium equations are derived from the first variation of (5)

$$\begin{aligned} &\delta\Pi_k(u_j, w_j, \psi_j, \lambda_{u_i}, \lambda_{w_i}, k_{yx}, k_{yy}) = 0, \\ &\quad \forall\{\delta u_j, \delta w_j, \delta\psi_j, \delta\lambda_{u_i}, \delta\lambda_{w_i}\}, \quad j = 1, \ldots, n_l + n_u, \;\; i = 1, \ldots, n_l + n_u - 1, \;\; i \neq n_l, \end{aligned} \tag{8}$$

valid for every cinematically admissible displacements. The variation with respect to Lagrange multipliers results in the following equations:

$$\begin{cases} w_j = w_{n_l} \quad j = 1, \ldots, n_l - 1, \\ w_j = w_{n_l+1} \quad j = n_l + 2, \ldots, n_l + n_u, \end{cases}$$

$$\begin{cases} u_j = u_{n_l} + \frac{t_{n_l}}{2}\psi_{n_l} + \sum_{k=j+1}^{n_l-1} t_k\psi_k + \frac{t_j}{2}\psi_j \quad j = 1, \ldots, n_l - 1, \\ u_j = u_{n_l+1} - \frac{t_{n_l+1}}{2}\psi_{n_l+1} - \sum_{k=n_l+2}^{j-1} t_k\psi_k - \frac{t_j}{2}\psi_j \quad j = n_l + 2, \ldots, n_l + n_u, \end{cases} \tag{9}$$

which allow the reduction to only $n_l + n_u + 4$ displacement variables, assumed to be

$$\{w_{n_l}, w_{n_l+1}, u_{n_l}, u_{n_l+1}, \psi_i (i = 1, \ldots, n_1 + n_u)\}. \tag{10}$$

Then, separating the domain into the two regions $x \in [0, a]$ and $x \in [a, L]$ and performing integration by parts gives local equilibrium equations, the related boundary ($x = a$) and matching conditions ($x = a$) for stress resultants and the analytical expressions of Lagrange multipliers. Expressions for the matching conditions and Lagrange multipliers can be found in Appendix A. From these formulas it can be noted that boundary and matching conditions ($x = a$) relative to arbitrary variations of section rotations, take into account for possible concentrated Lagrange multipliers acting as forces in the x-direction and arising due to a discontinuity in membrane force resultants. For instance, for the concentrated Lagrange multiplier at the ith interface we have

$$\lambda^c_{u_i} = \sum_{j=1}^{i} N_j \Big|_{x=0^+} - \sum_{j=1}^{i} \overline{N}_j, \quad \lambda^c_{u_i} = \sum_{j=1}^{i} N_j \Big|_{x=a^+} - \sum_{j=1}^{i} N_j \Big|_{x=a^-} \tag{11}$$

at $x = 0$ and at $x = a$, respectively (see Fig. 1). Strictly speaking, concentrated Lagrange multipliers arise only at the end of the sub-laminates ($x = 0$) due to possible stress singularities whereas at the delamination front stress singularities are excluded as far as the penalty parameters assume finite values. In the limit, as the penalty parameters approach infinity, stress singularities at the delamination front are reconstructed and concentrated Lagrange multipliers appear directly as a consequence of the limit procedure. Due to stress concentration at the delamination front as the penalty parameters approach infinity, the solution may change very rapidly near $x = a$. Moreover, due to the non-linearity of the interface law (3), numerical methods solving the two-point boundary value problem may suffer convergence difficulties. To avoid such inconveniences, the two-point boundary value problem has been described as two problems, one for $x \in [0, a]$ and the other one for $x \in [a, L]$, by using the appropriate matching conditions arising from the variational procedure.

4. Solution procedure and mode partition accuracy

The three-point boundary value problem governing the equilibrium of the delaminated composite structure subjected to end forces, can be reformulated as a non-linear system of first order ordinary differential equations subject to boundary conditions only at two-points. To this end, two separate sets of unknowns for the intervals $x \in [0, a]$ and $x \in [a, L]$, respectively, are introduced and a new independent natural variable ξ spanning both the intervals is adopted trough the relations:

$$\xi = \frac{x}{a} \quad x \in [0, a], \quad \xi = \frac{x - a}{L - a} \quad x \in [a, L]. \tag{12}$$

Consequently, the common variable ranges from 0 to 1. Note that matching conditions at $x = a$ become coupled boundary conditions for the reformulated differential problem, since they involve values of the solution at both ends of the interval $[0, 1]$. As a result, the reformulated boundary value problem assumes the form

$$\boldsymbol{y}'_k(\xi) = \boldsymbol{g}_k(\boldsymbol{y}_k, \xi), \quad 0 \leqslant \xi \leqslant 1, \tag{13}$$

where $\boldsymbol{y}_k = \{\boldsymbol{y}_1, \boldsymbol{y}_2\}^{\mathrm{T}}$ is a vector of the unknown functions of the problem (collecting displacement parameters and their derivatives), with $\boldsymbol{y}_1$ and $\boldsymbol{y}_2$ the row vectors corresponding to the interval $x \in [0, a]$ and $x \in [a, L]$, respectively. These vectors assume the form:

$$\boldsymbol{y}_i = \{w_{n_l}, w'_{n_l}, w_{n_l+1}, w'_{n_l+1}, u_{n_l}, u'_{n_l}, u_{n_l+1}, u'_{n_l+1}, \psi_1, \psi'_1, \ldots, \psi_{n_l+n_u}, \psi'_{n_l+n_u}\} \quad i = 1, 2. \tag{14}$$

$\boldsymbol{g}_k$ is an opportune vector function. In Eqs. (13) and (14) the prime denotes differentiation with respect to ξ. The subscript k denotes explicit dependence of the solution $\boldsymbol{y}$ from the penalty parameters. Eq. (13) is subjected to the two-point linear boundary conditions:

$$\boldsymbol{B}_0\boldsymbol{y}_k(0) + \boldsymbol{B}_1\boldsymbol{y}_k(1) = \boldsymbol{c}, \tag{15}$$

where $\boldsymbol{B}_0$ and $\boldsymbol{B}_1$ are opportune matrices containing coefficients of boundary and matching conditions and $\boldsymbol{c}$ is an opportune known vector depending on the applied forces. The two-point boundary value problem for fixed values of the penalty parameters, has been solved by means of an iterative collocation method implemented in MATLAB The Math Works Inc. (2000) which provides a C^1-continuous solution by using a cubic collocation polynomial on each subinterval of the mesh. Starting from an initial guess for the solution and the mesh, at each iteration the method adapts the mesh to obtain a sufficiently accurate numerical solution. The accuracy is measured by controlling the size of the residuals of numerical solution in both differential equations and boundary conditions. The solution satisfying both adhesion and contact constraints is obtained by means of a numerical limit procedure for discrete values of the penalty parameters, as

$$\boldsymbol{y} = \lim_{k_{yy},k_{yx}\to\infty} \boldsymbol{y}_k. \tag{16}$$

It is worth noting that each element of the sequence generated by the penalty procedure is in turn the result of a non-linear iteration process needed to satisfy the non-linear differential problem (13). For a faster convergence, in the numerical procedure the sliding and opening penalty parameters has been suitably calibrated to account for the evolution of interface relative displacements. Moreover, the use of different values for penalty parameters in the delaminated and undelaminated zones may be a good strategy to obtain a more efficient solution procedure. The penalty procedure has been terminated until the numerical solution has satisfied the following tolerance criterion based on the energy release rates:

$$\max\{eG_{\mathrm{I}}, eG_{\mathrm{II}}, eG_{\mathrm{T}}\} \leqslant 10^{-3}, \tag{17}$$

where eG_{I}, eG_{II} and eG_{T} represent the relative errors for energy release rate mode components and total energy release rate, respectively. Moreover, the tolerance criterion (17) was coupled with the following one

$$\frac{\Delta w_{n_l}(x)}{\sum_{i=1}^{n_l+n_u} h_i} > -\varepsilon \quad x \in \Omega_c, \tag{18}$$

to obtain a sufficiently accurate solution in the case when contact may occur. In numerical applications the value of ε was chosen to be no larger than 10^{-5}. For large values of the penalty parameters k_{yy} and k_{yx} the solution changes rapidly and a supposition good enough to represent this behavior must be adopted. To this aim a continuation technique in the penalty parameters is adopted, according to which the mesh and solution for one value of the penalty parameters is used as an initial supposition for larger values. The convergence behavior of computed values for energy release rates in the penalty procedure augmented by means of the continuation technique, is shown in Fig. 2 where a logarithmic scale (base 10) is used for the horizontal axis. The penalty parameters are assumed to be equal (i.e. $k_{yy} = k_{yx} = k$). The sub-laminates are considered as two equally isotropic homogenous plates with the following material and geometrical properties:

$$E_1 = E_2 = E = 70,000 \text{ MPa}, \quad \upsilon_1 = \upsilon_2 = 0.3, \ T = 0.1 \text{ N/mm}, \ a = 10 \text{ mm}, \tag{19}$$

and two end vertical opposite forces are applied. Each curve for both mode components and total energy release rate, corresponds to a uniform division of the upper and lower sub-laminates into n_u and n_l plate elements, respectively. Note that the total energy release rate does not depend on the sub-laminate division. From Fig. 2 it can be noted that for a low number of plate elements the total energy release rate has a convergence rate higher than that of the energy release rate mode components. Moreover, the convergence

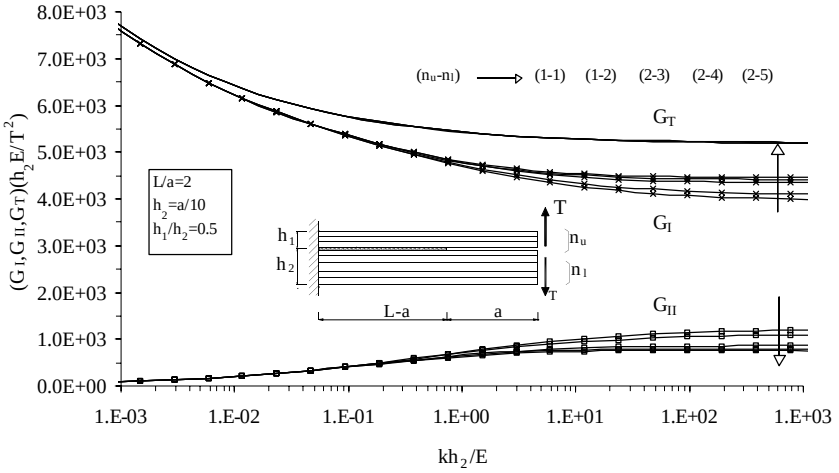

Fig. 2. Convergence of energy release rates in the penalty procedure as the number of plate elements in each sub-laminate increases: two opposite transverse shear forces. The arrows denote directions of refinement in sub-laminate division.

rate of the individual energy release rates increases as the division is refined and approximately both mode components and total energy release rate reach the same convergence rate.

The mode partition obtained by using the numerical solution (16) in formulas (2), is now compared to analytical results available in the literature based on two-dimensional continuum models. In particular, the solution provided by (Suo, 1990; Suo and Hutchinson, 1990) is adopted, valid when membrane and bending force resultants are applied at the laminate edge because is obtained by using the classic plate theory and the continuum approach. The classic double cantilever beam (DCB) scheme is examined for different thickness ratios. Results have shown that if sub-laminates are modeled by the same number of plate elements, refining uniformly sub-laminate division leads to a good agreement with Suo's results only when the delamination is located near the plate mid-plane (i.e. $h_1/h_2 \approx 1$). To obtain an accurate mode

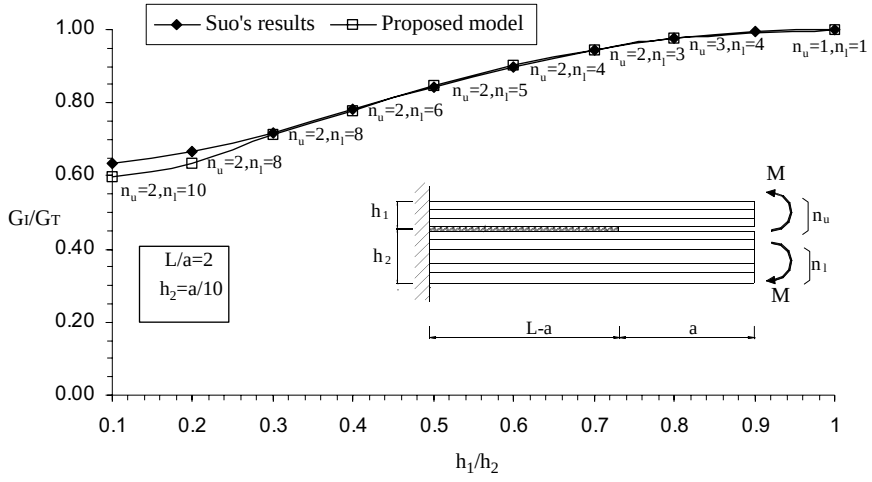

Fig. 3. Percentage of the total energy release rate for mode I energy release rate component, versus thickness ratio: validation of mode partition predicted by the proposed model by adopting a sub-laminate division according to the configuration of the delaminated plate.

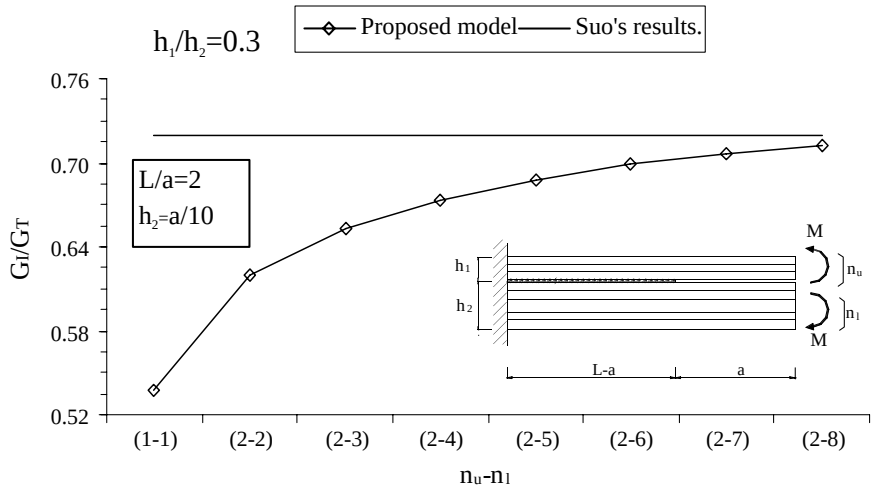

Fig. 4. Convergence of the proposed model as the number of plate elements increases for a fixed thickness ratio.

partition, sub-laminate division must reflect plate configuration, by using more plate elements on the thicker sub-laminate, as shown in Fig. 3. In these circumstances, results from the proposed model are in good agreement with Suo's results for all examined thickness ratios. As the thickness ratio decreases towards the thin film model, a more refined sub-laminate division is needed to capture the actual local delamination tip strain state. The relative energy release rates differences between our numerical results and Suo's are within 1%, except when the thickness ratio is less than 0.2. When $h_1/h_2 = 0.2$ the error is equal to about 5%, since the maximum refinement has been limited to 2 and 8, (2–8), plate elements for the upper and the lower sub-laminate, respectively, whereas for $h_1/h_2 = 0.1$ the error is less then 6% with a (2–10) sub-laminate division. Although results shown in Fig. 3 are limited to a thickness ratio of 0.1, additional numerical investigations have shown that the proposed model is efficient also for smaller values, if appropriate sub-laminate divisions are adopted. The convergence with respect to results obtained from continuum

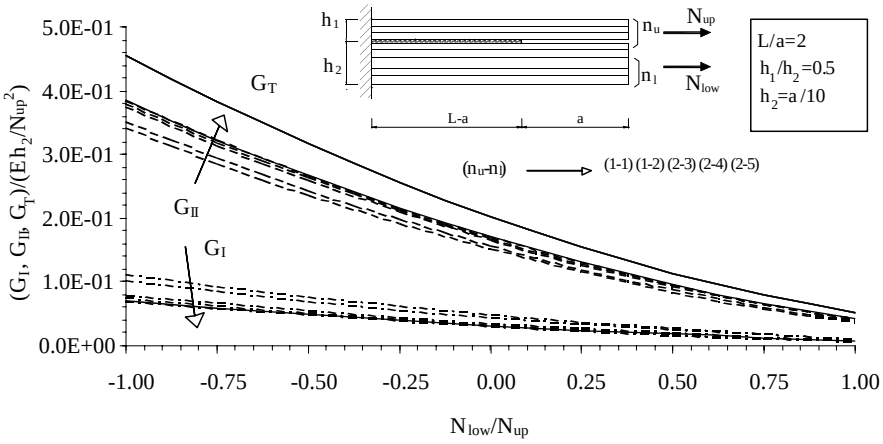

Fig. 5. Convergence of mode partition procedure for a pure membrane loading condition. Continuous curves are referred to Suo's results. The arrows denote directions of refinement in sub-laminate division.

analysis within the fixed thickness ratio $h_1/h_2 = 0.3$, is illustrated in Fig. 4. Results obtained for mode partition are also in a good agreement with those proposed by Zou et al. (2001). In addition, Point and Sacco (1996) proposing a two-layer plate model adopting classical plate theory, also noted differences in mode partition between results obtained by their model and by finite element solution of a continuum model. This shows that the classical two-layer delamination model is not appropriate for mode decomposition when $h_1 \neq h_2$. Several schemes have been considered for different loading cases leading to similar considerations. For instance, Fig. 5 show that for a pair of opposite axial forces, the curves representing Suo's results, shown in continuous lines, are in good agreement with those relative to the (2–5) sub-laminate division. It is worth noting that adopting a coarse subdivision in plate elements leads to overestimate the mode I energy release rate component, while the mode II one is underestimated. On the contrary, the total energy release rate is well approached also in the case of a rough subdivision.

5. Numerical applications

In this section some mixed mode delamination schemes will be analyzed, comparing results to solutions available in the literature and illustrating the capability of the proposed model to provide a realistic reconstruction of interlaminar stresses and of the local delamination front strain state.

5.1. Influence of shear deformability

Unfortunately, the solution obtained by using a local continuum analysis is restricted to the semi-infinite crack scheme under remote edge loading and is valid rigorously for sub-laminates of homogeneous orthotropic materials. Consequently, some approximations must be introduced in order to deal with practical laminate structures having a more complex lay-up and for which the classic plate theory is too approximated, since shear deformability effects cannot be neglected. On the contrary, as will be shown in the following, the proposed approach is able to avoid the above-mentioned inconveniences. To this end the influence of shear deformability on mode partition is now investigated. At first some numerical results are given to analyze the pure shear loading condition. Numerical results proposed in Fig. 6 show that a pure shear loading condition gives rise practically to only mode I energy release rate. This is in agreement with

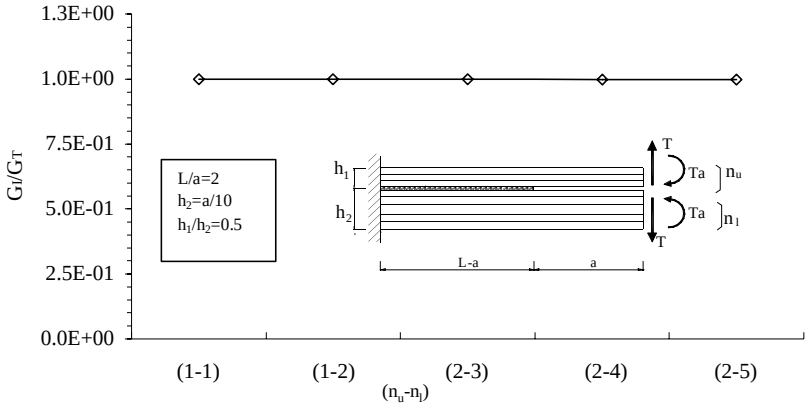

Fig. 6. Mode partition in pure shear loading condition.

the conclusions drawn by Williams (1988) and Nilsson et al. (2001a). The pure shear loading condition is simulated by eliminating bending effects trough a pair of moments opposite to those caused by the end shear forces at the delamination front sections.

Fig. 7 shows plots of both individual and total energy release rates for a delaminated plate of an isotropic homogeneous material having the same properties as the previous examples. Here results evidence that the global energy release rate is well predicted already when a single plate element is introduced to model each sub-laminate. On the other hand, the energy release rate mode I component increases as the plate element number increases, whereas the mode II component decreases. This implies that when the evaluation of shear deformability effects is improved, a better subdivision of energy release rate aliquots arising from bending effects is gained. As a matter of fact, contributions arising from pure shear being related to only the mode I energy release rate, are well evaluated also if a two-layer plate model is adopted and inaccuracies in mode partition are related mainly to contributions associated with bending moments. The convergence of mode partition procedure as the number of plate elements increases for end shear force loading is examined in Fig. 8, where a vertical section of plot in Fig. 7 relative to $T_{low}/T_{up} = -1$, is shown. Results for mode partition from the proposed model for different locations of delamination plane over the laminate thickness, are shown in Fig. 9. In particular for two equal and opposite shear forces as delamination moves away from the mid-plane the contribution to the mode II energy release rate increases. On the other hand, when the forces have the same direction mode I energy release rate increases. Finally the case of a E-Glass fibre/epoxy laminate with a cross-ply layup [0°/90°] with 18 plies, subjected to end shear forces, is considered. The upper sub-laminate has a $[0°/90°]_3$ layup, whereas the lower one a $[0°/90°]_6$ layup. Results concerning mode partition are presented in Fig. 10, whereas the convergence behavior fot two equal and opposite shear forces is illustrated in Fig. 11. A convergence behavior similar to that of Fig. 8 has been obtained. The mechanical properties of the unidirectional lamina are $E_{11} = 45{,}000$ MPa; $E_{22} = 12{,}000$ MPa; $v_{12} = 0.19$; $v_{21} = 0.274$; $G_{12} = 5,500$ MPa (the 0°-direction is parallel to the x direction).

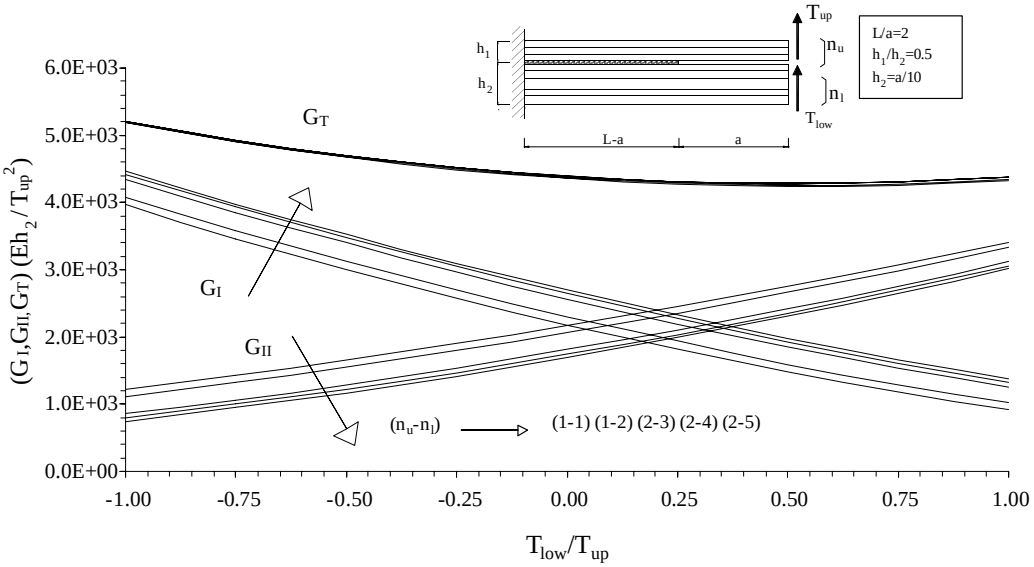

Fig. 7. Dimensionless energy release rates for different loading cases arising from two end shear forces: effects of sub-laminate division refinements. The arrows denote directions of refinement in sub-laminate division.

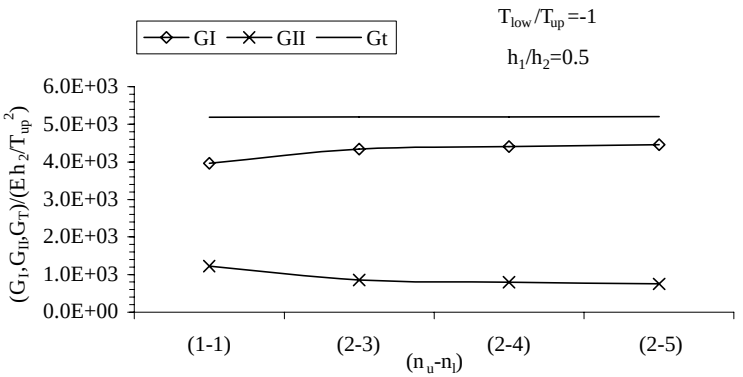

Fig. 8. Convergence of the mode partition procedure when $T_{\text{low}}/T_{\text{up}} = -1$ in the example considered in Fig. 7.

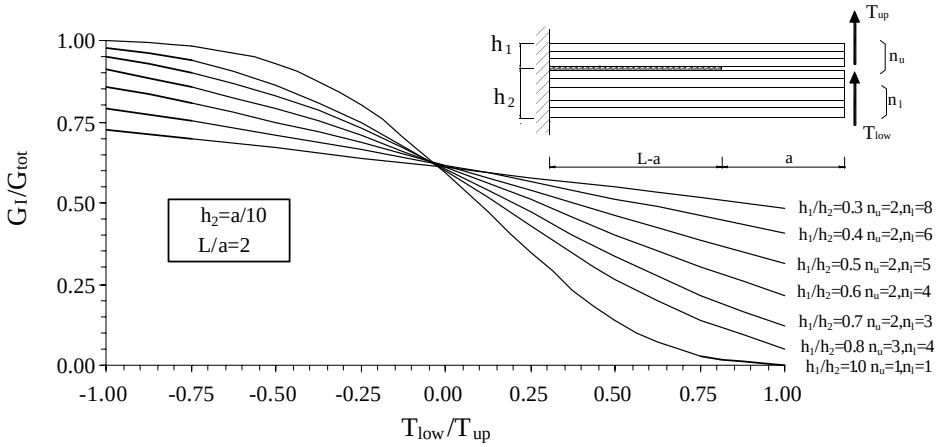

Fig. 9. Percentage of mode I energy release rate for the delamination scheme with end shear forces for different thickness ratios.

5.2. Comparison with classic delamination models

The objective of applications examined in this paragraph is to evidence how the proposed model is able to interpret the different levels of approximations in delamination analysis, and to show the notable differences between plate-based and continuum-based models, which are generally larger for orthotropic or composite materials than for isotropic material. Fig. 12 illustrates differences in mode partition between the two-layer plate model with shear stiffness approaching infinity (referred to as ''Kirchhoff'' model in Fig. 12), and the present model. The plate is made of an isotropic material with data from Eq. (19) and is subjected to two equal and opposite shear forces. Sub-laminate divisions used in Fig. 12 are shown in Table 1. The comparison with the above-discussed classic delamination model is now performed for three different laminates with the same geometrical parameters and different mechanical properties: the first (1) is composed of an homogeneous isotropic material, the second (2) is composed of an homogeneous orthotropic material and the third (3) by two different homogeneous orthotropic materials for the upper and lower sub-laminate. Table 2 shows the mechanical properties for the three examples: the last two assumes an E_1/G_{xy}^i ratio equal to 30. Table 3 shows the comparisons between classic and present models in terms of

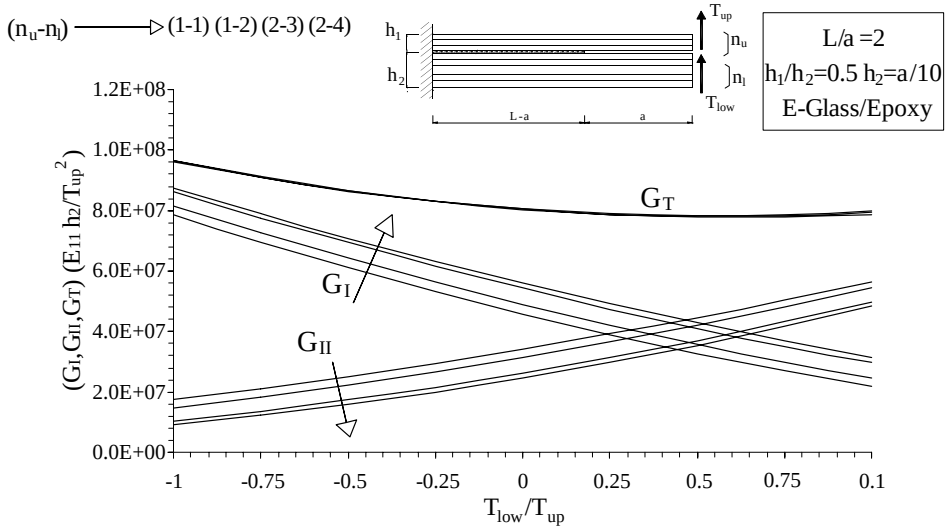

Fig. 10. Dimensionless energy release rates for different loading cases arising from two end shear forces in a E-Glass fibre/Epoxy laminates with a cross-ply layup: effects of sub-laminate division refinements. The arrows denote directions of refinement in sub-laminate division.

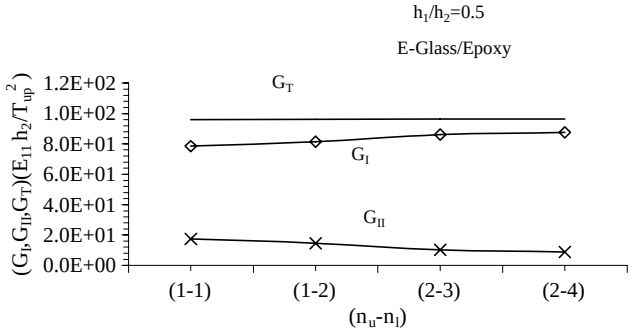

Fig. 11. Convergence of the mode partition procedure as sub-laminate division is refined, when $T_{low}/T_{up} = -1$ in the example considered in Fig. 10.

relative percentage differences for a delamination scheme loaded by two equal and opposite end shear forces. The thickness ratio h_1/h_2 is equal to 0.5 and sub-laminate division is assumed (2–5). For instance, for mode I this is evaluated as $| G_I^{class} - G_I^{present} | / G_I^{present}$%. The percentages of energy release rate mode components are shown in Table 4. Finally the effect of sub-laminate division on the differences between the classic and present model is illustrated in Fig. 13, showing only differences in individual modes increase as the division is refined. In this figure G_T, G_I, G_{II} refer to the present model whereas G_{TK}, G_{IK}, G_{IIK} to the Kirchhoff model.

As shown via numerical results the total energy release rate is noticeably underestimated as far as the two-layer Kirchhoff plate model is adopted, whereas it is well approached if each sub-laminate is modeled by one shear deformable plate element. On the contrary a good approximation in individual energy release rates requires also a refined sub-laminate division, since the mode I energy release rate component is always underestimated.

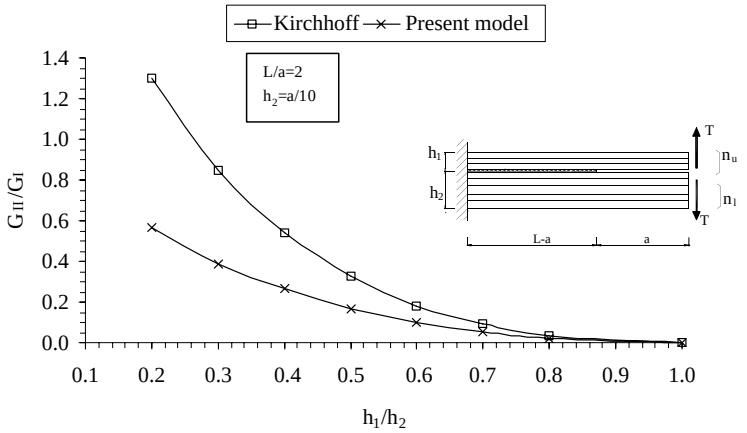

Fig. 12. Comparison between the proposed model and the Kirchhoff-based classic delamination model in terms of mode ratio. Isotropic material.

Table 1
Sub-laminate division in plate elements for the example in Fig. 12

h_1/h_2	0.2	0.3	0.4	0.5	0.6	0.7	0.8	1.0
$(n_u–n_l)$	(2–8)	(2–8)	(2–6)	(2–5)	(2–4)	(2–3)	(3–4)	(1–1)

Table 2
Mechanical properties of sub-laminates

Example	Upper sub-laminate				Lower sub-laminate			
	E_1 (MPa)	G^1_{xy} (MPa)	v^1_{xz}	v^1_{zx}	E_2 (MPa)	G^2_{xy} (MPa)	v^2_{xz}	v^2_{zx}
1	70,000	26,923	0.3	0.3	70,000	26,923	0.3	0.3
2	70,000	2,333	0.3	0.3	70,000	2,333	0.3	0.3
3	35,000	1,167	0.3	0.3	70,000	2,333	0.3	0.3

Table 3
Relative percentage differences between classic and present models

Example	G_I	G_{II}	G_T
1	16.0	63.6	4.5
2	28.0	68.8	16.1
3	33.1	41.3	13.8

Table 4
Individual energy release rate percentages for proposed and classic models

Example	Proposed model		Classical model	
	G_I/G_T	G_{II}/G_T	G_I/G_T	G_{II}/G_T
1	85.65	14.35	75.41	24.59
2	87.78	12.22	75.41	24.59
3	74.07	25.93	57.48	42.52

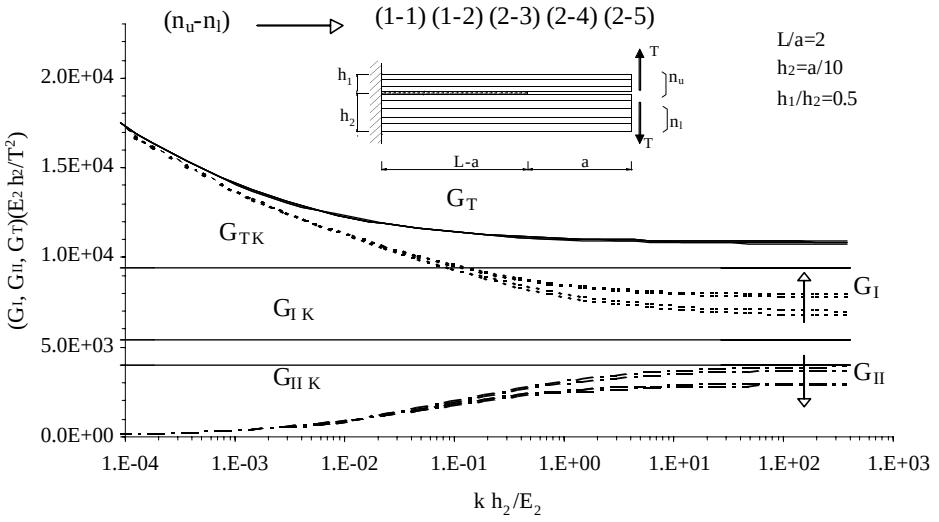

Fig. 13. Comparison between the proposed model and the classic delamination model in terms of individual and total energy release rates. Example 3: two different orthotropic materials. In the figure, the arrows denote directions of refinement in sub-laminate division.

6. Energy release rates and stress singularities

Analytical formulas are now obtained for both total and individual energy release rates in terms of delamination front stress resultant discontinuities, by applying the Griffith criterion and the virtual crack closure method (VCCM) to the present formulation based on interface and plate variables. The total energy release rate can be obtained by working in terms of plate element strain energies or interfacial quantities. According to the former approach, the energy release rate, calculated as:

$$G\dot{a} = -\frac{\mathrm{d}}{\mathrm{d}t}\Pi(u_i, w_i, \psi_i), \tag{20}$$

where Π is the limit of Π_k when the interface stiffness parameters approach infinity, after some algebraic calculations gives

$$G = \sum_{i=1}^{n_u+n_l}\left(\frac{1}{2}[\![N_i\varepsilon_i + M_i\kappa_i + T_i\gamma_i]\!]_a - [\![T_i]\!]_a\psi_i\right), \tag{21}$$

where the symbol $[\![f]\!]_a$ is specified in Appendix A, a point stands for partial differentiation with respect to time-like parameter t governing the monotonic growth of the delamination and $\mathrm{d}/\mathrm{d}t$ is the total time derivative. This is generalized version of the formula obtained in (Greco et al., 2002) for a two-layer plate model, and it can be expressed in terms of stress resultants by considering the constitutive relations. To obtain Eq. (21), it must be noted that the penalized version of the total potential energy Π_k must be evaluated along paths for the variables satisfying Eq. (8), and that the time derivative involves integration over two moving domains sharing the point $x = a$, which is the location of stress resultant discontinuities. The latter alternative is to extract discontinuities directly from the interface strain energy, starting from the regularized version of the total potential energy:

$$G\dot{a} = -\lim_{k\to\infty}\frac{\mathrm{d}}{\mathrm{d}t}\Pi_k(u_i, w_i, \psi_i), \tag{22}$$

where the limit procedure is performed for penalty parameters accounting for adhesion, thus leading to

$$G = -\lim_{k\to\infty}[\![\Lambda + \sigma_{yy}\Delta w_{n_l} + \sigma_{yx}\Delta u_{n_l}]\!]_a = \lim_{k_{yx},k_{yy}\to\infty}\frac{1}{2}(k_{yy}\Delta w_{n_l}^2 + k_{yx}\Delta u_{n_l}^2). \tag{23}$$

Eqs. (21) and (23) show the relation between the stress singularities causing finite limit values in interface strain energy terms and stress resultant discontinuities which avoid dealing directly with stress singularities. The latter approach, however, does not determine mode partition that, on the contrary, is obtained immediately from Eq. (23). It is worth noting that, as shown by previous numerical simulations, the use of more than two elements provides a refinement at the level of mode partition, but not for the total energy release rate prediction. As a matter of fact, a crucial improvement in energy release rate determination is obtained by using two plate elements instead of one in the undelaminated region, since in the latter case contributions to the energy release rate arising from the last term in Eq. (21), vanish, causing a notable underestimation of shear effects.

According to VCCT the energy released into individual modes is half the work performed by delamination front point Lagrange multipliers (see Fig. 14b) before the delamination is advanced by da through separations occurring after the delamination is extended by da (see Fig. 14a):

$$G_{\mathrm{I}} = \frac{1}{2\mathrm{d}a}\lambda^c_{w_{n_l}}\Delta w_{n_l}, \quad G_{\mathrm{II}} = \frac{1}{2\mathrm{d}a}\lambda^c_{u_{n_l}}\Delta u_{n_l}, \tag{24}$$

where the expressions for Lagrange multipliers and separations are included in Appendix B. Utilizing adhesion constraint and constitutive relationships (see Eqs. (B.3)–(B.5) in Appendix B), after some algebraic manipulations leads to the following formulas:

$$G_{\mathrm{I}} = \sum_{i=1}^{n_u+n_l}\left(\frac{1}{2}[\![T_i\gamma_i]\!]_a - [\![T_i]\!]_a\psi_i\right), \quad G_{\mathrm{II}} = \sum_{i=1}^{n_u+n_l}\left(\frac{1}{2}[\![N_i\varepsilon_i + M_i\kappa_i]\!]_a\right). \tag{25}$$

The above results provide interesting analytical formulas for individual energy release rate components. A possible advantage of using Eq. (25), consists in avoiding more than one stress analysis of the delaminated plate needed to apply the VCCT, since individual modes can be extracted directly from stress resultant discontinuities.

Eq. (25) show that shear deformability directly affects mode I energy release rate component since is related only to jumps in shear stress resultants and strains at the crack tip, while mode II arises from jumps in membrane and bending quantities at the crack tip. To gain better insight into this latter point, for

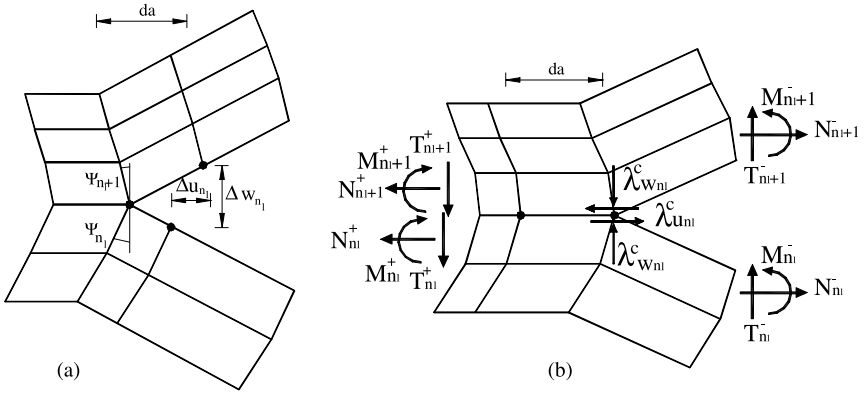

Fig. 14. Virtual crack closure method representation in the present model: (a) separations scheme; (b) closing forces scheme.

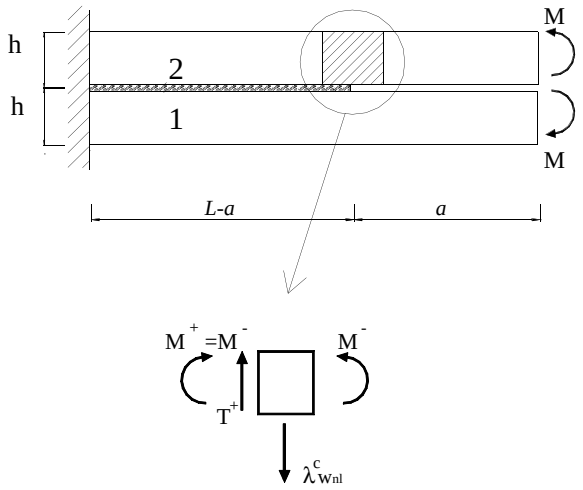

Fig. 15. Symmetrical DCB scheme with opening moments and illustration of Lagrange multiplier and stress resultants at the delamination tip.

instance, the symmetrical DCB scheme composed of two equal orthotropic materials and subjected to opening moments shown in Fig. 15, can be considered. For the sake of simplicity, a double plate model ($n_u = n_l = 1$) is adopted for this example. In this case no jumps in bending moment resultants occur at the crack tip and thus according to Eqs. $(25)_2$ G_{II} vanishes, whereas jumps in shear stress resultants, related to the presence of a vertical point Lagrange multiplier, cause a non-zero G_{I} (see also Bruno and Greco, 2003). As a matter of fact (see Fig. 15) since T at $x = a^-$ is equal to zero, due to equilibrium requirements at $x = a^+$, T (denoted as T^+) is equal to the point Lagrange multiplier $\lambda^c_{w_{n_l}}$:

$$T^+ = H(w' + \psi)|_{x=a^+} = \lambda^c_{w_{n_l}}.$$

In view of the fact that w' at $x = a^+$ is equal to zero due to adhesion constraint, then

$$T^+ = H\psi|_{x=a^+} = \lambda^c_{w_{n_l}}.$$

Using results obtained in Eq. (20) of (Bruno and Greco, 2001a) for $(L-a)/h \to \infty$, we obtain

$$\psi|_{x=a^+} = \psi|_{x=a^-} = -\frac{M}{\sqrt{HD}} = \frac{T}{H},$$

and applying Eq. $(25)_1$ leads to

$$G_{\mathrm{I}} = 2\left(\frac{1}{2}[\![T_2\gamma_2]\!]_a - [\![T_2]\!]_a\psi_2\right) = \left[\!\left[\frac{T_2^2}{H}\right]\!\right]_a - 2[\![T_2]\!]_a\frac{T}{H} = \left.\frac{T^2}{H}\right|_{a^+} = \frac{M^2}{D}.$$

In the previous equations H and D denote the shear and bending stiffnesses of the two equal plates, respectively.

A further understanding of the effectiveness of Eq. (25) can be gained by examining the results shown in Fig. 6, where a pure shear loading condition gave rise only to the mode I energy release rate. To prove this it is sufficient to consider that Eq. $(B.2)_2$, due to constitutive relations (4), furnishes a zero relative sliding displacement, when only shear stress resultants act on sections behind the delamination front and belonging to plate elements adjacent to the delamination plane (i.e. $M_i = N_i = 0$, $i = n_l, n_l + 1$). As a consequence, it is

evident that inaccuracies in energy release rate evaluation obtained by adopting a classic delamination model evidenced in Figs. 12 and 13, are related to an underestimation of the mode I energy release rate.

7. Delamination and contact

Numerical simulations are now performed to assess the efficiency of the combined interface/multilayer approach for delamination analysis of laminates accounting for crack–face interactions due to contact. Some practical problems are considered to verify the performance of the proposed model and to analyze the influence of contact between delaminated members on delamination growth features.

At first, a homogeneous plate containing a mid-plane delamination is considered. The two delaminated elements are loaded by two opposite moments so that crack face interpenetration occurs if contact constraint is not incorporated into the analysis. A two-layer plate modeling is adopted due to the mid-plane symmetry about the delamination plane. Fig. 16 shows the behavior of the opening relative interface displacement in the penalty procedure: the contact area is decreasing under external loading and contact tends to be maintained in a single point at the ends of the delaminated members. In Fig. 17 the total energy release rate is shown as the penalty parameters approach infinity, revealing the good convergence behavior of the proposed method. In this example the choice of equal values for penalty parameters simulating adhesion and contact was adopted. Attention is now focused on the laminate considered in Fig. 13, composed of two different orthotropic materials and subjected to two equal end moments leading to contact between delamination faces. Two and five plate elements are incorporated in the analysis for the upper and lower sub-laminates, respectively, and equal values for penalty parameters related to sliding and opening interface displacements are adopted. As shown in Fig. 18, the overlapping region decreases as the penalty procedure advances and tends toward a point. The situation is somewhat similar to the previous example but features involved both in the deformation process and in the numerical analysis are more variegated. For instance, in order to make the numerical procedure more efficient the penalty parameters for adhesion and contact have been increased with different rates, once a threshold value of $kh_2/E_2 = 0.05$ is

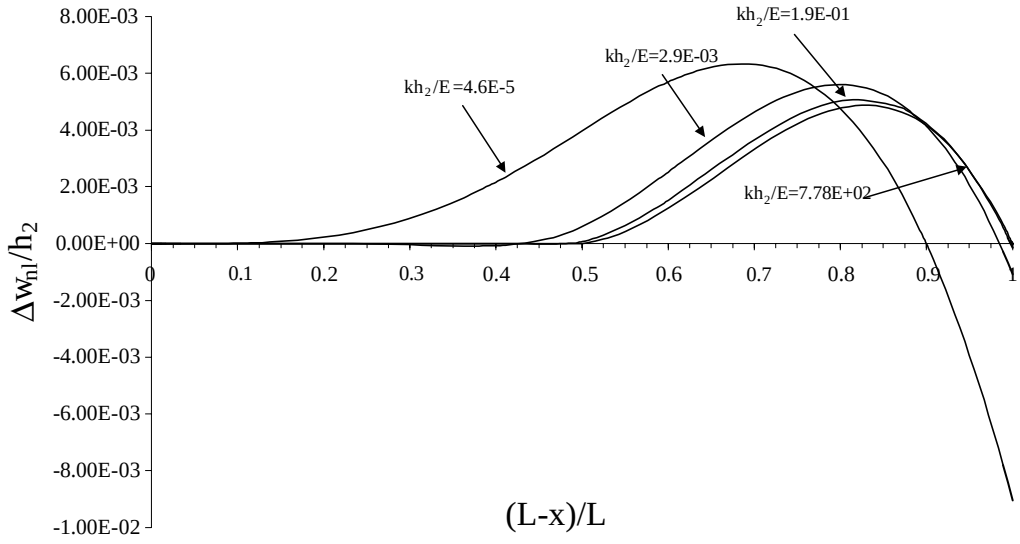

Fig. 16. Relative opening interface displacement function as a function of the non-dimensional distance from the clamped end, for a plate containing a symmetric located delamination.

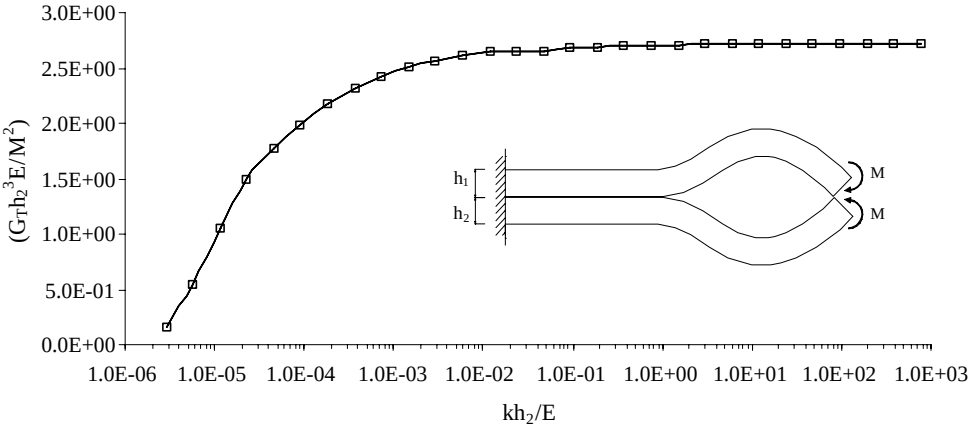

Fig. 17. Energy release rate behavior during the penalty procedure.

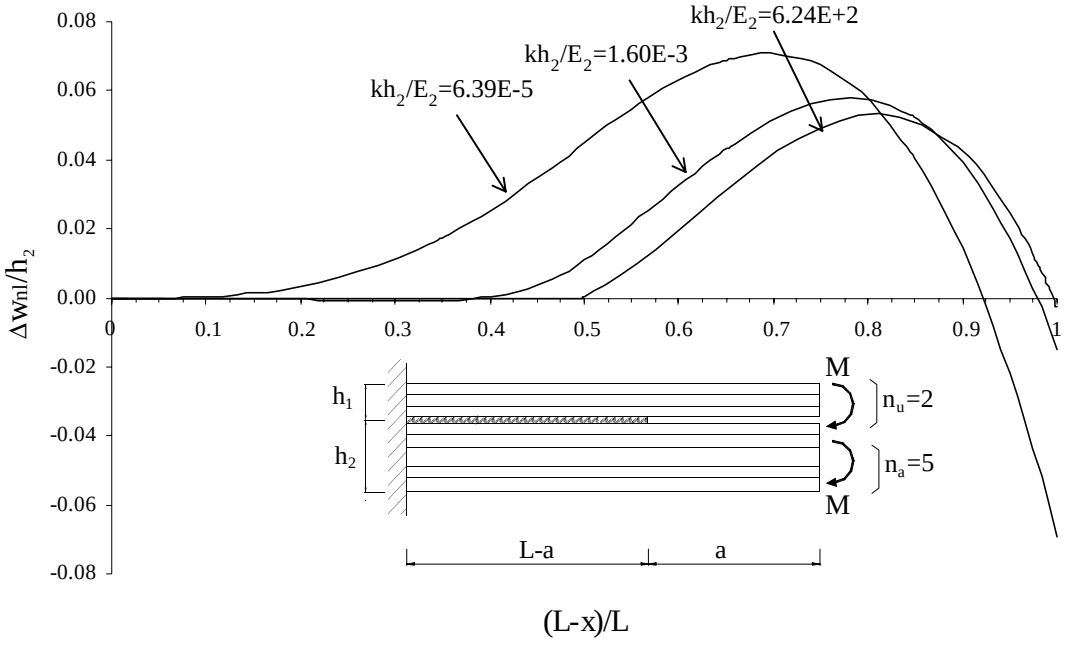

Fig. 18. Laminate composed of two different orthotropic layers coming into contact: ratio $\Delta w_{n_l}/h_2$ versus $(L-x)/L$ for different values of penalty parameters. $n_u = 2$, $n_l = 5$.

reached. This ensures a smooth behavior of numerical values for energy release rates, since the satisfaction of the contact condition disturbs the convergence of fracture energies during the numerical penalty procedure. In addition, satisfaction of the contact and adhesion conditions occur at larger values of penalty parameters with respect to the previous example. The final admissible configuration for the delaminated plate is shown in Fig. 19 together with the physically inadmissible configuration arising if contact is not taken into account. For the case without contact analysis, the upper sub-laminate penetrates into the lower one. The convergence of the total energy release rate and of its mode components is investigated in Fig. 20,

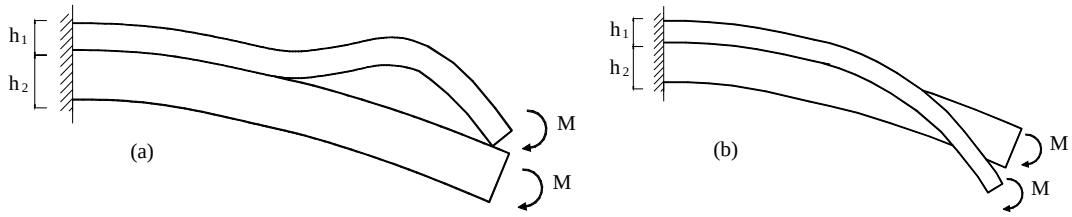

Fig. 19. Deformation modes for the delaminated laminate made of two different orthotropic layers: (a) actual mode; (b) inadmissible mode.

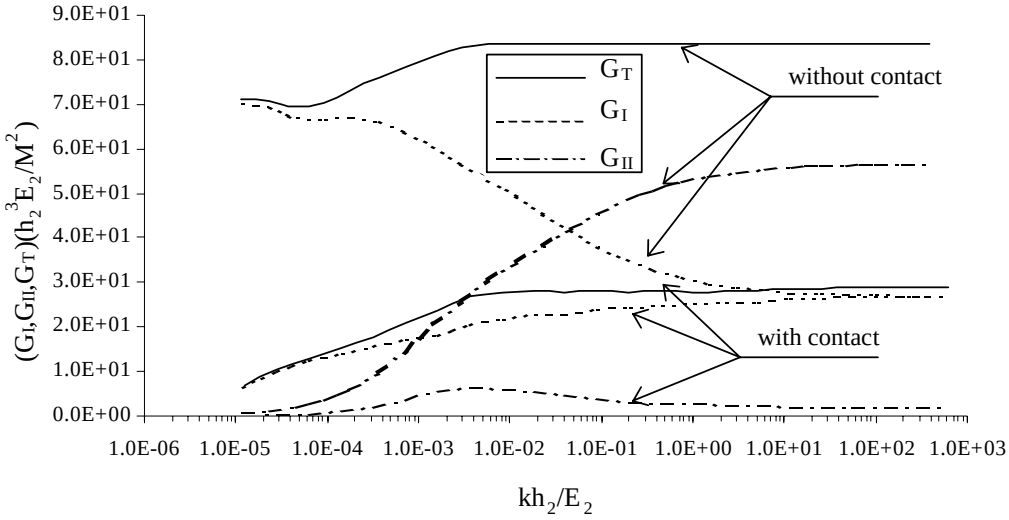

Fig. 20. Total energy release rate and individual mode components as a function of penalty parameters when contact is analyzed and when contact is not taken into account.

where, in addition, deviations of numerical results without contact analysis when compared with the case obtained including contact, are illustrated. When contact is taken into account the energy release rates decrease since the deformation mode requires greater strain energy. Moreover, the thicker sub-laminate is forced by the thinner one to deflect and, as a consequence, the mode I energy release rate component is greater than the mode II one, a situation opposed to the analysis without contact. Note that the mode I energy release rate component corresponds to a co-penetration at the delamination front ($\Delta w < 0$), and this should be considered as zero according to Eq. (2). Nevertheless, Fig. 20 shows both mode components in order to compare the mechanical behavior of the laminate in the two different analyses.

These results shown that contact analysis is inevitable for analyzing some loading configurations in a delaminated plate. Finally, the above numerical studies show the ability of the proposed model to account also for non-linear interface laws. Consequently it is expected that the present model will perform well for more complex circumstances such as laminates containing multiple delaminations when delaminated members often may often come into contact. In this case, the use of the proposed multilayer plate modeling, which well simulates well the three-dimensional behavior at the delamination front, may avoid the anomalous discontinuity behavior of energy release rate detected in previous investigations utilizing classic plate modeling (see, for instance, Larsson, 1991).

8. Conclusions

A laminate model based on multilayer shear deformable plate modeling and interface elements is proposed to analyze mixed mode delamination. Interface elements, based on fracture mechanics and contact mechanics, are introduced along the delamination plane to simulate perfect bonding and to prevent the interpenetration of delaminated members.

The coupling of a penalty procedure with the Lagrange multiplier method, used to enforce displacement continuity between plate elements away from the delamination plane, results in an accurate and direct energy release rate evaluation. Comparison with results available from the literature obtained with the continuum approach, shows that the proposed model is capable of capturing the different levels of approximations in delamination analysis by refining sub-laminate division in plate elements, ranging between the extreme cases of classical delamination models and the continuum-based models. Furthermore, original analytical results are obtained with respect to mode partition, which are useful to evidence the effectiveness of the proposed approach and to gain a better insight into the influence of shear effects on mode decomposition.

The most notable advantages detected in the present investigation of two-dimensional delaminated structures, are here evidenced:

- it may avoid complicated computations based on solid finite element analyses and not convenient from the engineering point of view, which may become very expensive for complex delamination problems (multiple delaminations, interface contact, bridging, composite laminates with general ply-stacking sequence);
- the complications related to oscillatory behavior of energy release rates are avoided through the use of interface and plate variables;
- it provides an effective mode decomposition accurately incorporating shear effects;
- the proposed method may be utilized to include several kinds of non-linear interlaminar behavior (such as bridging, strain-softening damage laws, etc), as well as crack face interaction due to contact, which must be accounted for to analyze progressive delamination occurring frequently during the post-delamination phase.

The previous considerations underline that the model analyzed in the current work, represents an effective bond between classic fracture mechanics concepts and interface approaches coupled with laminate theory, and show the effectiveness of the model to deal accurately with two-dimensional mixed mode delamination problems, while retaining the advantages of a plate-based approach.

Appendix A

Lagrange multipliers arising from interface displacement continuity requirement, assume the following expressions:

$$\lambda_{u_i} = \sum_{j=1}^{i} N'_j = \sum_{j=1}^{i} A_j \left(u''_{n_l} + \frac{t_{n_l}}{2}\psi''_{n_l} + \sum_{k=j+1}^{n_l-1} h_k \psi''_k + \frac{t_j}{2}\psi''_j \right) + \sum_{j=1}^{i} B_j \psi''_j \quad i = 1, \ldots, n_l - 1,$$

$$\lambda_{u_i} = -\sum_{j=i+1}^{n_l+n_u} N'_j = -\sum_{j=i+1}^{n_l+n_u} A_j \left(u''_{n_l+1} - \frac{t_{nu}}{2}\psi''_{n_l+1} - \sum_{k=n_l+2}^{j-1} h_k \psi''_k - \frac{t_j}{2}\psi''_j \right) - \sum_{j=1}^{i} B_j \psi''_j$$
$$i = n_l + 1, \ldots, n_l + n_u - 1,$$

$$\lambda_{w_i} = \sum_{j=1}^{i} T'_j = \sum_{j=1}^{i} H_j(w''_{n_l} + \psi'_j) \quad i = 1, \ldots, n_l - 1,$$

$$\lambda_{w_i} = -\sum_{j=i+1}^{n_l+n_u} T'_j = -\sum_{j=i+1}^{n_l+n_u} H_j(w''_{n_l+1} + \psi'_j) \quad i = n_l + 1, \ldots, n_l + n_u - 1, \tag{A.1}$$

where a prime denotes differentiation with respect to x. The stress resultants matching conditions are given as follows

$$\begin{aligned}
&\left[\!\left[\sum_{j=1}^{n_l} N_j \right]\!\right]_a = \left[\!\left[\sum_{j=n_l+1}^{n_l+n_u} N_j \right]\!\right]_a = 0, \quad \left[\!\left[\sum_{j=1}^{n_l} T_j \right]\!\right]_a = \left[\!\left[\sum_{j=n_l+1}^{n_l+n_u} T_j \right]\!\right]_a = 0,\\
&\left[\!\left[M_1 + N_1 \frac{t_1}{2} \right]\!\right]_a = \left[\!\left[M_{n_l} + \sum_{j=1}^{n_l-1} N_j \frac{t_j}{2} \right]\!\right]_a = 0, \quad \left[\!\left[M_i - \left(\sum_{j=1}^{i} N_j + \sum_{j=1}^{i-1} N_j \right) \frac{t_i}{2} \right]\!\right]_a = 0 \quad i = 2, \ldots, n_l - 1,\\
&\left[\!\left[M_{n_l+1} - \sum_{j=n_l+2}^{n_l+n_u} N_j \frac{t_{n_l+1}}{2} \right]\!\right]_a = \left[\!\left[M_{n_l+n_u} - N_{n_l+n_u} \frac{t_{n_l+n_u}}{2} \right]\!\right]_a = 0,\\
&\left[\!\left[M_i - \left(\sum_{j=i+1}^{n_l+n_u} N_j + \sum_{j=i}^{n_l+n_u} N_j \right) \frac{t_i}{2} \right]\!\right]_a = 0 \quad i = n_l + 2, \ldots, n_l + n_u - 1,
\end{aligned} \tag{A.2}$$

where $[\![f]\!]_a$ denotes the jump $f^- - f^+$ occurring at $x = a$ in the enclosed function, with the superscripts + and – denoting that the function is evaluated at $x = a^+$ and $x = a^-$, respectively. Similar expressions can be obtained for the boundary conditions of stress resultants.

Appendix B

The point Lagrange multipliers, reflecting singularities in normal and shear interface stresses in the limit as interface stiffness parameters approach infinity, are evaluated as:

$$\lambda^c_{w_{n_l}} = -\left[\!\left[\sum_{j=1}^{n_l} T_j \right]\!\right]_a = \left[\!\left[\sum_{j=n_l+1}^{n_u+n_l} T_j \right]\!\right]_a, \quad \lambda^c_{u_{n_l}} = -\left[\!\left[\sum_{j=1}^{n_l} N_j \right]\!\right]_a = \left[\!\left[\sum_{j=n_l+1}^{n_u+n_l} N_j \right]\!\right]_a, \tag{B.1}$$

whereas the corresponding interlaminar separations can be expressed as:

$$\Delta w_{n_l} = \left(\frac{T^-_{n_l+1}}{H_{n_l+1}} - \frac{T^-_{n_l}}{H_{n_l}} + \psi_{n_l+1} - \psi_{n_l} \right) \mathrm{d}a, \quad \Delta u_{n_l} = \left(u'^-_{n_l+1} + \psi'_{n_l+1} \frac{t_{n_l+1}}{2} - u'^-_{n_l} + \psi'_{n_l} \frac{t_{n_l}}{2} \right) \mathrm{d}a, \tag{B.2}$$

where all quantities are evaluated at the delamination front. For the mode I computation, due to the perfect adhesion hypothesis between adjoining plate elements, it follows that

$$w'^+_{n_l} - w'^+_{n_l+1} = 0 \tag{B.3}$$

and, consequently,

$$\left(\frac{T^+_{n_l+1}}{H_{n_l+1}} - \frac{T^+_{n_l}}{H_{n_l}} \right) = \psi_{n_l+1} - \psi_{n_l}, \tag{B.4}$$

by virtue of the constitutive relationships. Eq. (B.4) allows to write Eq. $(B.2)_1$ in terms of shear stress resultants discontinuities. On the other hand, the VCCT application for mode II needs the following equations:

$$\Delta u'^{+} = \left(u'^{+}_{n_l} - \psi'^{+}_{n_l}\frac{t_{n_l}}{2}\right) - \left(u'^{+}_{n_l+1} + \psi'^{+}_{n_l+1}\frac{t_{n_l+1}}{2}\right) = 0, \tag{B.5}$$

which allows to express Eq. $(B.2)_2$ in terms of jumps in membrane strains and curvatures.

References

Allix, O., Corigliano, A., 1996. Modelling and simulation of crack propagation in mixed-modes interlaminar fracture specimens. Int. J. Fract. 77, 111–140.

Allix, O., Ladevèze, P., Corigliano, A., 1995. Damage analysis of interlaminar fracture specimens. Compos. Struct. 31, 61–74.

Ascione, L., Bruno, D., 1985. On the delamination problem of two-layer plates. Proceedings of the Second Meeting on Unilateral Problems in Structural Analysis, Ravello, 22–24 September, 1983, CISM Courses and Lectures No. 288, Springer, Berlin.

Bruno, D., Greco, F., 2000. An asymptotic analysis of delamination buckling and growth in layered plates. Int. J. Solids Struct. 37, 6239–6276.

Bruno, D., Greco, F., 2001a. Delamination in composite plates: influence of shear deformability on interfacial debonding. Cement Concr. Compos. 23 (1), 33–45.

Bruno, D., Greco, F., 2001b. Mixed mode delamination in plates: a refined approach. Int. J. Solids Struct. 38/50–51, 9149–9177.

Bruno, D., Greco, F., 2003. An efficient model of mixed-mode delamination in laminated composites including bridging mechanisms. Simulat. Modell. Pract. Theor. 11, 465–481.

Bui, V.Q., Marechal, E., Nguyen-Dang, H., 2000. Imperfect interlaminar interfaces in laminated composites: interlaminar stresses and strain—energy release rates. Compos. Sci. Technol. 60, 131–143.

Chai, H., Babcock, C.D., Knauss, W.G, 1981. One dimensional modelling of failure in laminated plates by delamination buckling. Int. J. Solids Struct. 17 (11), 1069–1083.

Cochelin, B., Potier-Ferry, M., 1991. A numerical model for buckling and growth of delaminations in composite laminates. Comput. Meth. Appl. Mech. 89, 361–380.

Davidson, B.D., Hurang, H., Schapery, R.A., 1995. An analytical crack-tip element for layered elastic structures. J. Appl. Mech. 62, 294–305.

Greco, F., Lonetti, P., Zinno, R., 2002. An analytical delamination model for laminated plates including bridging effects. Int. J. Solids Struct. 39, 2435–2463.

Hutchinson, J.W., Suo, Z., 1992. Mixed mode cracking in layered materials. In: Hutchinson, J.W., Theodore, Y.W. (Eds.), Advances in Applied Mechanics, vol. 28. Academic Press, New York, pp. 63–191.

Kim, J.-K., 1997. Postbuckling analysis of composite laminates with a delamination. Comput. Struct. 26 (6), 975–983.

Kouchakzadeh, M.A., Sekine, H., 2000. Compressive buckling analysis of rectangular composite laminates containing multiple delaminations. Compos. Struct. 50, 249–255.

Larsson, P.-L., 1991. On multiple delamination buckling and growth in composite plates. Int. J. Solids Struct. 27 (13), 1623–1637.

Nilsson, K.-F., Asp, L.E., Alpman, J.E., Nystedt, L., 2001a. Delamination buckling and growth for delamiantions at different depths in a slender composite panel. Int. J. Solids Struct. 38, 3039–3071.

Nilsson, K.-F., Asp, L.E., Sjogren, A., 2001b. On transition of delamination growth behavior for compression loaded composite panels. Int. J. Solids Struct. 38, 8407–8440.

Point, N., Sacco, E., 1996. Delamination of beams: an application to the DCB specimen. Int. J. Fract. 70, 225–247.

Raju, J.S., Crews Jr., J.H., Aminpour, M.A., 1988. Convergence of strain energy release rate components for edge-delaminated composite laminates. Eng. Fract. Mech. 30, 383–396.

Schapery, R.A., Davidson, B.D., 1990. Prediction of energy release rate for mixed-mode delamination using classical plate theory. Appl. Mech. Rev. 43, S281–S287.

Storåkers, B., Andersson, B., 1988. Nonlinear plate theory applied to delamination in composites. J. Mech. Phys. Solids 36 (6), 689–718.

Suo, Z., 1990. Delamination specimen for othotropic materials. J. Appl. Mech. 57, 627–634.
Suo, Z., Hutchinson, J.W., 1990. Interface crack between two elastic layers. Int. J. Fract. 43, 1–18.
The MathWorks Inc.: Using MATLAB, (Version 6). 3 Apple Hill Drive, Natick, MA, 2000.
Williams, J.G., 1988. On the calculation of energy release rate for cracked laminates. Int. J. Fract. 36, 101–119.
Zou, Z., Reid, S.R., Soden, P.D., Li, S., 2001. Mode separation of energy release rate for delamination in composite laminated using sublaminates. J. Solids Struct. 38, 2597–2613.